

Microbubble-microplastic interactions in batch air flotation

Swart Bert, Pihlajamäki Arto, Chew Y.M. John, Wenk Jannis

This is a Publisher's version version of a publication
published by Elsevier
in Chemical Engineering Journal

DOI: <https://doi.org/10.1016/j.cej.2022.137866>

Copyright of the original publication:

© 2022 The Author(s). Published by Elsevier.

Please cite the publication as follows:

Swart, B., Pihlajamäki, A., Chew, Y.M.J., Wenk, J. (2022). Microbubble-microplastic interactions in batch air flotation. Chemical Engineering Journal, vol. 449. DOI: 10.1016/j.cej.2022.137866

**This is a parallel published version of an original publication.
This version can differ from the original published article.**



Microbubble-microplastic interactions in batch air flotation

Bert Swart^{a,b,c}, Arto Pihlajamäki^d, Y.M. John Chew^{a,e,*}, Jannis Wenk^{a,b,*}

^a Department of Chemical Engineering, University of Bath, Bath BA2 7AY, UK

^b Water Innovation and Research Centre, University of Bath, BA2 7AY, UK

^c GW4 Water Informatics Science and Engineering (WISE) EPSRC Centre for Doctoral Training, Centre for Water Systems, University of Exeter, EX4 4PY, UK

^d Department of Separation Science, School of Engineering Science, LUT University, 53850 Lappeenranta, Finland

^e Centre for Advanced Separations Engineering, University of Bath, Bath BA2 7AY, UK

ARTICLE INFO

Keywords:

Bubble size distribution
Image processing
Microbubbles
Rise velocity
Surfactants

ABSTRACT

Presence of microplastics in waste streams and the environment is a challenge of much recent concern. Bubbles are used for solid–liquid separation in froth flotation and dissolved air flotation (DAF). Bubble-particle interactions are key for understanding flotation removal efficiency of particulates. Limited studies provide in-situ characterization of particle size distribution, shape and concentration before and after flotation. The use of microbubbles to specifically remove microplastics has not been extensively investigated. This study presents a batch flotation method to assess the removal of spherical polyethylene (PE) and non-spherical PE, polypropylene (PP), polyvinyl chloride (PVC), and polymethyl methacrylate (PMMA) microplastic of different densities at 10–600 μm size range with 50–110 μm sized microbubbles. In-situ image analysis allowed measuring particle shape, size and concentration in solution prior to and after flotation as well as capturing particle-bubble interactions at the micro-scale. Besides determining flotation performance for different microplastic sizes, shapes and types, the effect of surfactant concentration and ionic strength was investigated and discussed in relation to particle collection efficiency. This study provides important quantitative results on bubble-particle interaction that allow selective removal of microplastic from solution and presents a straightforward direct in-situ visualization method for tracking and characterizing micrometer-sized particles in solid–liquid-gas multiphase media.

1. Introduction

Microplastics (MPs) are plastic particles between 0.1 μm –5 mm in diameter [1,2]. MPs are ubiquitously present in the environment, especially in marine and freshwater systems [3–9]. MPs can have various negative effects on animals, microorganisms, plants and whole ecosystems through external physical effects or via disruption of internal physiological processes after ingestions, and as vector of chemical contaminants and pathogens [10–15].

MPs in the environment can be classified as primary or secondary origin [16]. Primary include MPs in personal care products, plastic pellets, synthetic textiles and breakdown of tires, road markings and marine coatings [3,17,18]. Secondary MPs are fragments of initially larger plastics broken down by physical, chemical and/or biological processes after release into the environment [2,19]. The shape and type of environmental MPs varies and includes particles, flakes, films and fibres [20–23]. Globally, the bulk of environmental MP is derived of only

a few different parent polymers but local composition can vary greatly [21,24–26].

Major pathways of MPs into the environment comprise accidental and unintentional discharge, mismanaged waste and waste water streams [27–29], including waste water treatment plants (WWTPs) [30]. Solids separation processes applied in WWTPs after primary clarification and activated sludge treatment can achieve 95–99% MP removal [25]. However, a key concern with WWTPs is the potential release of MPs to the environment through distribution on land via biosolids produced in activated sludge treatment [30] and release of separated solids [26] from primary clarification to landfills. MPs contained in wastewater effluent may have only a small contribution to environmental plastic [31]. In addition, MPs can cause operational issues, performance decline and equipment damage in WWTPs [28,29].

Flotation of suspended solids with bubbles has been widely used for water clarification and solids recovery [32,33] including for plastics recycling (Supplementary Information [SI], Table S1) [34,35]. In a typical flotation process, suspended particles attach to rising bubbles of

* Corresponding authors at: Centre for Advanced Separations Engineering, Department of Chemical Engineering, University of Bath, Bath BA2 7AY, UK (Y.M. John Chew). Water Innovation and Research Centre, Department of Chemical Engineering, University of Bath, Bath BA2 7AY, UK (J. Wenk).

E-mail addresses: y.m.chew@bath.ac.uk (Y.M. John Chew), j.h.wenk@bath.ac.uk (J. Wenk).

<https://doi.org/10.1016/j.cej.2022.137866>

Received 8 May 2022; Received in revised form 25 June 2022; Accepted 29 June 2022

Available online 2 July 2022

1385-8947/© 2022 The Author(s). Published by Elsevier B.V. This is an open access article under the CC BY license (<http://creativecommons.org/licenses/by/4.0/>).

Nomenclature			
u	Bubble or particle rise/settling velocity	u_b	Bubble rise velocity
d	Bubble or particle equivalent diameter	μ	Fluid dynamic viscosity
ρ	Bubble or particle density	κ	Inverse Debye length
ρ_l	Liquid density	r	Particle radius
g	Gravitational acceleration	ϵ_r	Dielectric constant
μ	Fluid dynamic viscosity	ϵ_0	Permittivity of free space
Re	Reynolds number	k_B	Boltzmann constant
τ_p	Characteristic particle reaction time	T	Absolute temperature
τ_b	Characteristic time of fluid solicitation	N_A	Avogadro's number
ρ_p	Particle density	e	Elementary charge
d_p	Particle diameter	I	Ionic strength electrolyte of solution
d_b	Bubble diameter	MB	Microbubble
		MP	Microplastic

size 1–4 mm (macro-bubbles) and the resulting aggregates and froth can be removed from the liquid surface [36–38]. Microbubbles (MBs, 1–100 μm) compared to macro-bubbles can increase flotation performance significantly [39]. Theoretical studies on MB-particle interaction including on collection efficiencies, particle/bubble shape, size and surface properties effect on flotation performance have been carried out [40–43]. Additionally, experimental MB flotation studies using various materials (Table S2) [44–49] are also available. However, few studies investigated using MBs to specifically separate and remove MPs from water and those which have, did not fully validate and verify both MB and MP measured diameters with in-situ image analysis [50,51]. Previous studies on MB-particle interactions have used non-specific analysis such as turbidity and optical absorbance measurements or time-consuming gravimetric methods to quantify flotation performance with minimal in-situ visualization and tracking of MBs and MP particles (Table S2). Experimental investigation of specific effects of particle shape and size on particle-bubble interaction have only been studied on stationary macro-bubbles [52–54]. An increased understanding of MP-MB interaction could aid developing specific MP separation, for example at different stages of wastewater treatment processes, especially in WWTPs not designed for the mitigation of MPs.

The aim of this study was to investigate MB flotation of MPs in water to understand the interaction between MP particle sizes, shapes, number density and types with rising MBs. Removal of MPs from water using batch dissolved air flotation (<2 min flotation time), with a narrow size distribution of MB diameters of 60–115 μm , was investigated for different surfactant and ionic concentrations. In addition to addressing a research gap on MP-MB interaction, this manuscript presents a robust, fast and repeatable batch flotation procedure. An image analysis method utilizing in-house MATLAB code allowed for in-situ MB and MP visualization, tracking and measuring of MP number density, without need for prior MP separation, for comparative analysis, including size and shape distribution before and after flotation.

2. Materials & methods

2.1. Materials

Deionized (DI) water from a reverse osmosis system (Purite Integra HP120GP, Suez Water Technologies & Solutions, Berkshire, UK) was used for experiments and preparation of stock solutions, all unbuffered. Non-ionic surfactant polyethylene glycol sorbitan monolaurate (Tween-20), NaCl, MgCl_2 , $\text{Al}_2(\text{SO}_4)_3 \cdot 16\text{H}_2\text{O}$ and $\text{AlK}(\text{SO}_4)_2 \cdot 12\text{H}_2\text{O}$ were from Merck, Darmstadt, Germany. Spherical polyethylene (PE) particles of diameters (10–600 μm) and densities (0.960–1.05 g cm^{-3}) were purchased from Cospheric, Santa Barbara, CA, USA. An electric sander (Bosch Orbital Sander PSS 250 AE) equipped with different grades of sanding paper (60–120) was used to generate MP particles from four types of plastic

sheets: high density polyethylene (PE), polypropylene (PP), polyvinyl chloride (PVC), and polymethyl methacrylate (PMMA) with densities of 0.955, 0.905, 1.380 and 1.180 g cm^{-3} respectively (theplasticshop.co.uk, Coventry, UK). Choice of plastic types for this study was based on environmental occurrence (PE and PP, [21,24–26]), to cover a range of densities and commercial availability of plastic sheets. Procedures for MP particle zeta potential measurement are provided in SI, Text S1.

2.2. Microbubble (MB) generation

A Nikuni KTM 20 N (Nikuni Co., Kawasaki City, Kanagawa, Japan; Aeration & Mixing LTD, Sheffield, UK) regenerative turbine pump was used to produce MB solution. The Nikuni pump was operated at manufacturer recommended parameters of – 0.03 MPa inlet pressure, 0.3 MPa outlet pressure, liquid flow rate of 16.5 L min^{-1} and an ambient air intake of 1.5 L min^{-1} . The setup is illustrated in Fig. 1a and described in detail in a previous publication [55]. MB solution was generated in a continuous loop by drawing DI water from a temperature-controlled (15–20 °C) water bath. MB solution for flotation experiments was diverted from the loop via a controllable needle valve.

2.3. Batch flotation

MP suspension was created by adding 0.4–0.5 g L^{-1} of spherical or sanded MP particles to DI water. Tween-20 was added at 12% of its critical micelle concentration (CMC = 0.06 mM), which was the minimum concentration needed to achieve wetting of MP particles. Batch MP flotation tests were carried out in a cylindrical flotation column (Height = 30 cm, Diameter = 4 cm, Volume = 350 ml). First, the initial MP suspension was decanted into the flotation column, filling up 50% or 75% of its volume. MB solution was then added via the needle inlet valve at a flowrate of approximately 2.5 L min^{-1} until the flotation column was 100% filled, creating a well-mixed solution of MP particles and MBs. Experiments with 50% volume of initial plastic suspension and MB solution each is referred to as 1:1 dilution, while those with 75% initial plastic suspension volume and 25% MB solution is referred to as 3:1 dilution. After a flotation time of approximately 2 min, after which all bubbles rose to the surface of the flotation column, the foamy MP/MB aggregates were skimmed off the surface. The remaining mixture in the flotation column is referred to as post-flotation sample. The post-flotation sample was decanted into a container and stored for image analysis. For each flotation experiment a control experiment was carried out by following the same procedure as for flotation experiments, but instead of MB solution, clear DI water was used to fill the remainder of flotation column. This corresponding solution is referred to as the control sample and was also stored for image analysis (Fig. 1b).

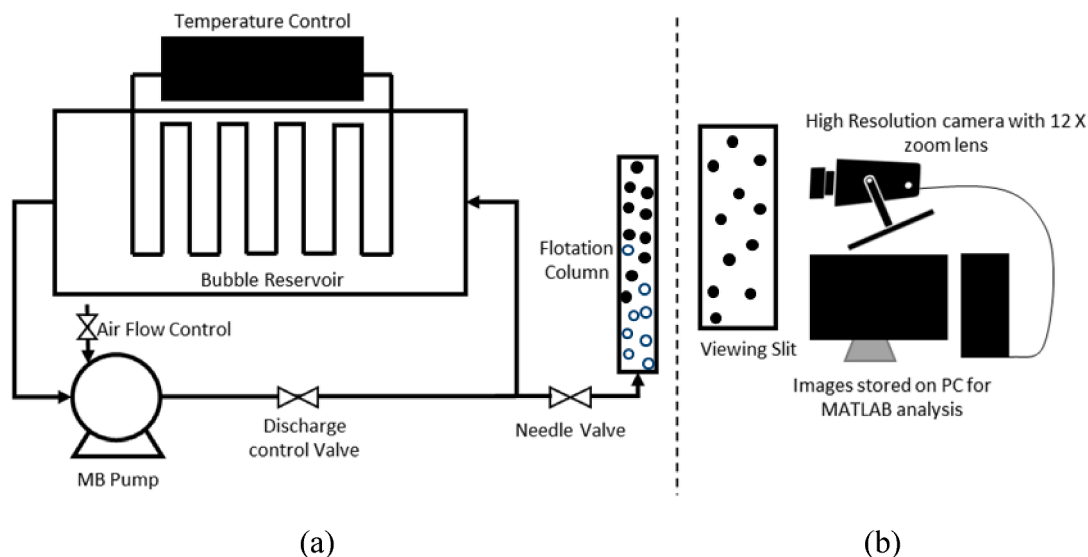


Fig. 1. Schematic of (a) microbubble generation loop and flotation column, and (b) viewing slit and image analysis.

2.4. Image capturing and processing for MP and MP/MB interactions

Images were captured by decanting the initial MP suspension, control or post-flotation sample into a clear PMMA viewing slit (Height = 13.5 cm, Width = 11.5 cm, Depth = 1 cm, thickness of PMMA = 3 mm). Examples of two initial MP suspensions can be seen in Fig. 2. For each sample, 100 images were captured with a Thorlabs DCU224C camera (Thorlabs, United States) with adjustable Navitar 12 × zoom lens (Navitar, United States) at five frames per second. To ensure no skewing of size distribution by random variance 100 images were taken per measurement. Improvement in accuracy of recorded size distribution beyond that number was negligible. The camera was mounted on a purpose-built adjustable support system to ensure that position and distance from the viewing slit (5–10 cm) could be accurately controlled and directed at the center of the viewing slit. A backlight system (Nightsearcher Galaxy Pro) at 10 cm distance from viewing slit ensured sufficient contrast. A scale image was taken before each experiment to be used when converting MP particle diameters from pixel width to μm (Fig. S1).

MP particle number density and size was determined using a bespoke image analysis algorithm via MATLAB. For both MP and MB analysis,

which was done separately, a previously described and validated image analysis procedure initially developed for MB analysis [55] was used to characterize particle and bubble size, shape and number density. Identification of particles and bubbles was based on the exclusion of image objects via threshold binarizing by Otsu's method [56] and minimum intensity of object. Binarizing the image singles out particles by eliminating background image via inclusion/exclusion decisions based on pixel darkness. The binarization factor required ranged from 0.4 to 0.6. Minimum intensity includes/excludes based on object darkness. The minimum intensity factor required ranged from 50 to 80. For irregular MP particles, particle diameter was calculated by converting the cross-sectional area into the equivalent diameter of a sphere with the same cross-sectional area. Analysis was also carried out to determine the shape of irregular particles via aspect ratio measurements. A lower size limit of 10 μm for particle identification of was set. Whilst identification of particles smaller than this is possible with the described methodology, it was determined that counts below this size are prone to error due to the faint appearance of such particles at the magnification used. Higher magnification captured particles smaller than 10 μm but reduced the number of particles recorded in size range of 10–500 μm that was the focus in this work. Measurement of particles smaller than 1 μm would

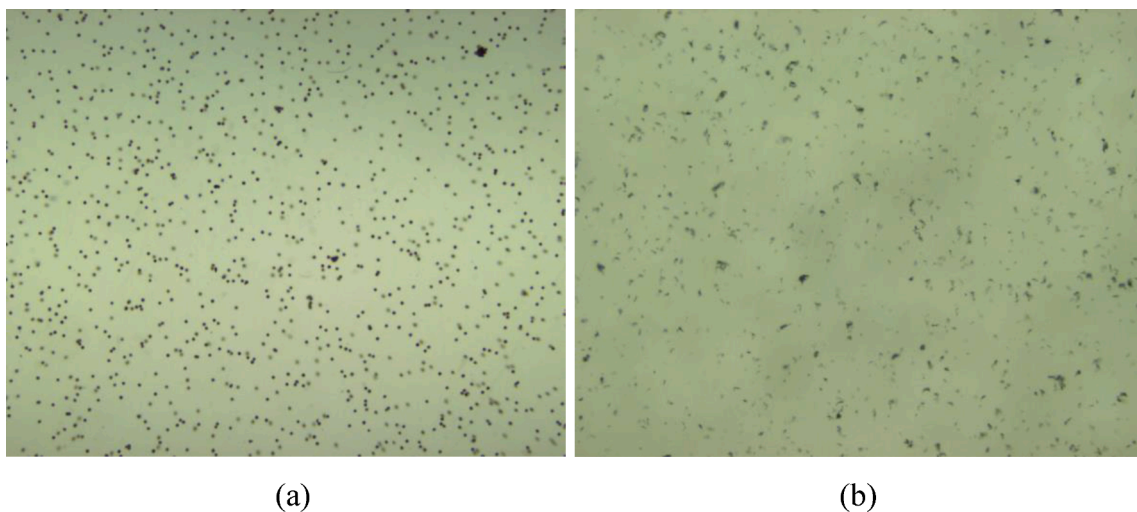


Fig. 2. Examples of images of initial 0.5 g L⁻¹ MP suspensions used for image analysis in MATLAB. (a) spherical PE MP particles 53–63 μm . (b) Irregularly shaped sanded PE MP particles. (Imaging window, w = 10.7 mm, h = 8.6 mm).

require a different imaging setup, likely microscope analysis.

Overall removal percentage was calculated by comparing particle counts in the post-flotation sample to that of the control sample. The use of image analysis to determine MP removal percentage was validated gravimetrically as described in detail in Text S2. For image analysis of the attachment of MBs to MP particles in solution, an identical experimental setup was used with a taller PMMA viewing slit Height = 50 cm (compared to 13.5 cm for other experiments). For these experiments MB solution was directly added through a bottom inlet at the viewing slit to a MP suspension to allow observation of particle interaction.

3. Theory

MBs in water can be assumed to behave as solid spherical particles of the same size and density, given their small size and low rise velocity [57]. At sufficient distance for unhindered movement both bubble spheres and particles motion are controlled by buoyancy force, the density difference between sphere and fluid, and the drag force, due to form drag and skin friction at the sphere surface. The resulting rise or settling velocity and flow regime can be described by the Stokes' equation and the particle/bubble Reynolds number,

$$u = \frac{d^2(\rho - \rho_l)g}{18\mu} \quad 1$$

$$Re = \frac{\rho_l u d}{\mu} \quad 2$$

where u is the bubble rise or particle settling velocity, d is the bubble/particle equivalent diameter, ρ is the bubble/particle density, ρ_l is the fluid density, g is the gravitational acceleration constant, μ is the fluid dynamic viscosity. MBs, with diameters 10–120 μm in 20 °C water, rise according to Stokes' equation with bubble Reynolds numbers in the creeping flow regime below 0.95 [55,57].

The key factors determining particle-bubble collection efficiency in flotation are illustrated in Fig. 3 I-IV [58,59]. The probability of interception (Fig. 3 I) is the likelihood of individual particles intercepted by the path of a rising bubble. It is determined by both the size of particles and bubbles and the number density of bubbles in solution. Modelling of particle-bubble trajectories considered both particles and bubbles rotation, but concluded that it has no effect on the relative translational velocity between particles and bubbles [43]. For a given bubble number density, greater particle and bubble size will result in increased interception. For a given particle and bubble size, increased bubble number density will result in increased interception.

Collision efficiency (Fig. 3 II) is the ratio of particles which collide with an intercepting bubble and is determined by the trajectory of particles around a rising bubble. The trajectory is determined by

hydrodynamic and interparticle forces and dictates whether particles are deflected or collide with rising bubbles. Note, Brownian motion is only significant for particles below 1 μm [40,43,58]. The inertial behaviour of a particle within moving fluid can be characterized by the Stokes' number [60]. According to the Stokes' number, when the characteristic particle reaction time, τ_p , is less than the characteristic time of fluid sollicitation, τ_b , due to bubble induced flow, the motion of a particle in the fluid around bubbles is non-inertial, meaning that particles follow the fluid streamlines around a bubble if no interparticle forces are present [61].

$$\tau_p = \frac{\rho_p d_p^2}{18\mu} \ll \tau_b = \frac{d_b}{2u_b} \quad 3$$

where, ρ_p is particle density, d_p is particle diameter, μ is the fluid dynamic viscosity, d_b is bubble diameter, u_b is bubble rise velocity. Calculations for parameters relevant in this study show non-inertial motion occurs with particles interacting with rising bubbles, with inertial behavior only expected when $d_p > 400 \mu\text{m}$. Particle bubble hydrodynamic calculations can be seen in Table S3. At approach, a particle and bubble exert a compressive force on the fluid between them. This results in repulsive hydrodynamic forces on bubble/particle couples causing deviation from fluid streamlines which can cause deflection of the particle from the bubble surface. Generally, for large size differences, flotation efficiency greatly reduces due to deflection of small particles around fast rising large bubbles or deflection of small bubbles around fast settling large particles. In addition to hydrodynamic forces, electric double layers at bubble/particle surfaces typically exercise repulsive electrostatic forces between the two. The dimensionless inverse Debye length Kr , which represents the inverse thickness of the electrical double layer multiplied by particle radius layer is given by,

$$Kr = r \left[\sqrt{\frac{\epsilon_r \epsilon_0 k_B T}{2N_A e^2 I}} \right]^{-1} \quad 4$$

where K is the inverse Debye length, r is the particle radius, ϵ_r is the dielectric constant, ϵ_0 is the permittivity of free space, k_B is the Boltzmann constant, T is absolute temperature, N_A is the Avogadro's number, e is the elementary charge and I is the ionic strength of electrolyte solution [62]. A full table of Kr calculations for conditions relevant to this study can be seen in Table S4. In addition, attractive van der Waals forces and long range hydrophobic interaction act between particles and bubbles [36]. The trajectories and collision efficiency of particles and MBs has been modelled considering hydrodynamic, electrostatic and van der Waals forces and plotted for various cases [43]. In summary, for a given bubble and particle size with the same zeta potential sign, collision is more likely at low zeta potential and a thin electric double layer. At these conditions electrostatic forces are small enough or

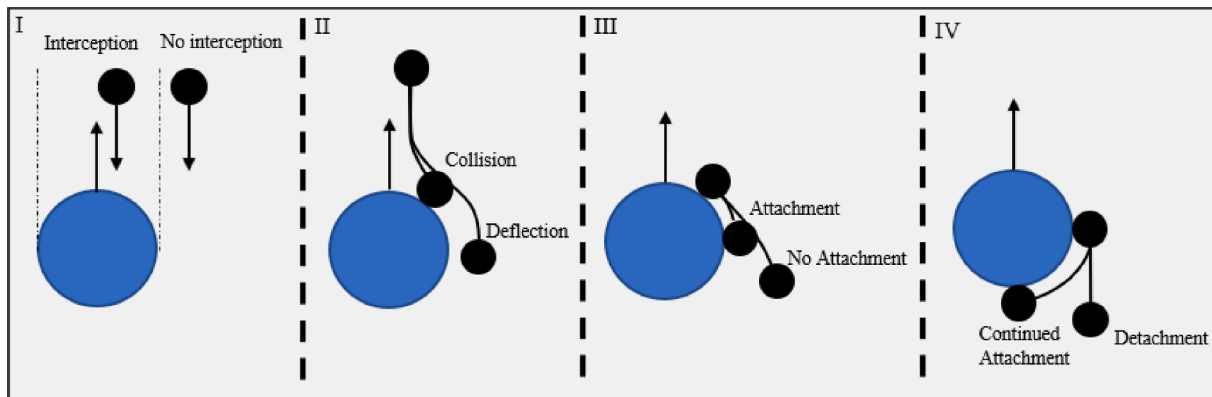


Fig. 3. Illustration of particle trajectory relative to a rising bubble and the four phases which determine collection efficiency. I: Likelihood of interception, II: Collision efficiency, III: Attachment efficiency, IV: Detachment rate.

operate over a small enough distance such that attractive van der Waals forces dominate.

Attachment efficiency (Fig. 3 III) is the proportion of colliding particles which attach to the bubble after collision occurs. There can be two types of particle-bubble attachment. The first is when a three-phase wetting perimeter is formed at the bubble and particle surface. At critical separation distance, the fluid film between bubble and particle is spontaneously ruptured. This type of attachment is driven by the hydrophobic force that correlates to the contact angle formed between particle and bubble, which is effected by both liquid surface tension and particle surface properties [52]. The second type of attachment, contactless flotation, occurs when attractive interparticle forces between a particle and bubble negate repulsive interparticle and hydrodynamic forces acting on the particle such as form drag, surface drag and negative buoyancy [58]. There is little mention of entrainment in major reviews and mathematical modelling of dissolved air flotation [36,40,43]. Research has shown that entrainment plays a small role in flotation performance for dissolved air/MB flotation, and removal is predominantly based on attachment between particle flocs and MBs [46].

Detachment rate (Fig. 3 IV) is the proportion of particles which detach after initial attachment. Detachment is affected by gravitation, inertia and turbulent conditions. Detachment can also be caused by subsequent collision with other bubbles or particles. For MB-MP aggregates, detachment is much less likely than for larger particles and bubbles [58]. Inertial and gravitational effects are proportional to particle volume and therefore have a greatly reduced effect on small particles [52]. Additionally, the rise and settling velocities are much smaller for micro sized particles and bubbles which result in greatly reduced turbulent forces and detachment.

4. Results and discussion

4.1. Characterization of microbubbles

Examples of bubble size distribution and cumulative frequency obtained from 100 images of a single experimental run are shown in Fig. 4. MBs used for flotation experiments were within 59–113 μm in diameter (90% frequency, measured in triplicate with 100 images per measurement), with mean bubble diameter varying from 72 to 87 μm . Air volume concentration in the MB solution, determined via change in solution volume with and without bubbles, was 5.25 ml of air per 1 L of air. Therefore, at 1:1 dilution and 3:1 dilution, air volume concentration is 2.65 ml L⁻¹ and 1.31 ml L⁻¹. Bubble number density in MB solution, ranged from 15,000–20,000 bubbles mL⁻¹. Therefore, at 1:1 dilution and 3:1 dilution, bubble number density in the flotation column was approximately 7500–10,000 bubbles mL⁻¹ and 3750–5000 bubbles

mL⁻¹ respectively. Bubble hydrodynamics are discussed elsewhere [55]. A previous study utilizing laser diffraction measured nanobubbles of diameters 0.05–0.4 μm produced by regenerative turbine pump [63]. In this study the presence of nanobubbles was not investigated as such bubbles would have negligible impact on flotation performance due to extremely low rise velocities and buoyancy.

4.2. Imaging of microbubble attachment to spherical PE microplastic particles

Image analysis was carried out to capture MB-MP particle attachment using spherical PE particles to determine whether attachment occurs predominantly via formation of a three-phase wetting perimeter or via contactless flotation. Fig. 5 a-d shows typical examples of rising bubble-particle aggregates. Almost all bubble-particle aggregates formed a three-phase wetting perimeter with a clear contact angle (Fig. 5 a-c). Fig. 5d shows a rising aggregate exhibiting little or no contact angle. Therefore, for spherical PE particles both contact and contactless flotation occurs, while the latter is less frequent (based on non-quantitative manual image analysis). The predominance of contact flotation is due to the hydrophobicity of PE causing attractive hydrophobic forces between particles and bubbles including film rupture between the particle-bubble surfaces. Images also confirmed no deformation of the bubbles typical for MBs which behave similarly to solid spheres in solution [57]. MB-MP collision also occurred without sustained attachment Fig. 5 e-h. Here, the bubble made brief contact with the particle and then continued to rise, while inducing a spin to the particle. These examples illustrate the potential of the employed in-situ image and video analysis for straightforward micrometer scale particle-bubble interactions visualization.

4.3. Effect of particle density and surfactant on removal by flotation

Particle density can have a significant effect on collision efficiency and attachment via changes in buoyancy and relative velocity towards bubbles. Flotation tests with spherical PE particles, with added surfactant (Tween 20) and different density were performed (Table 1). Increasing particle density from 0.96 to 1.05 g cm⁻³ decreased removal from 85% to 66%. This was expected since increased particle settling and relative velocity (Table 1) between MPs and MBs leads to decreased interaction time and increased repulsive hydrodynamic forces and deflection between bubbles and particles.

Changes to surface properties of MP particles are important for collection efficiency as it can alter hydrophobicity and electrostatic forces [64]. Increasing surfactant concentration from 0.12 to 0.36 CMC decreased removal of PE spheres (0.995 g cm⁻³) by 26% and 17% for the

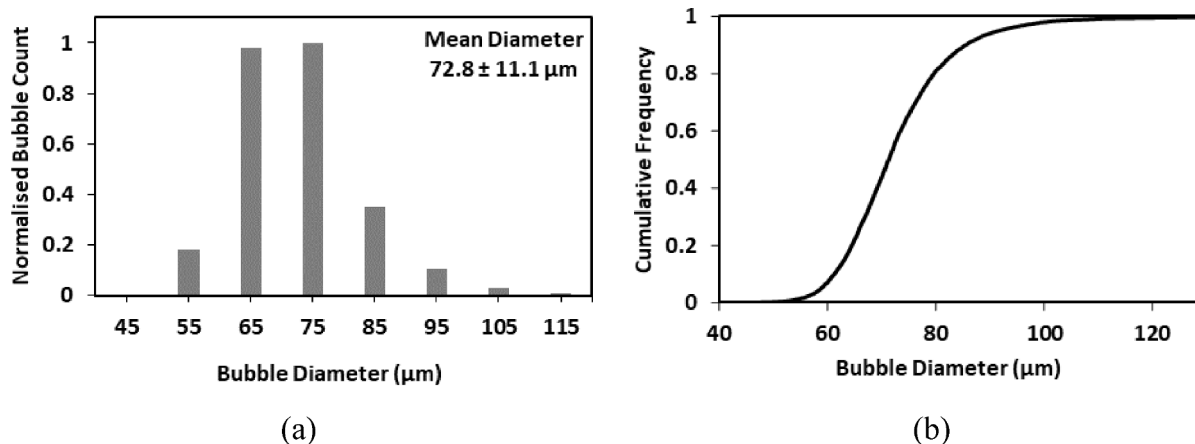


Fig. 4. (a) Bubble size distribution of bubbles (bin size: $\pm 5 \mu\text{m}$) used for flotation experiments with mean bubble diameter ± 1 standard deviation displayed and (b) normalized cumulative frequency of bubble sizes used for flotation experiments.

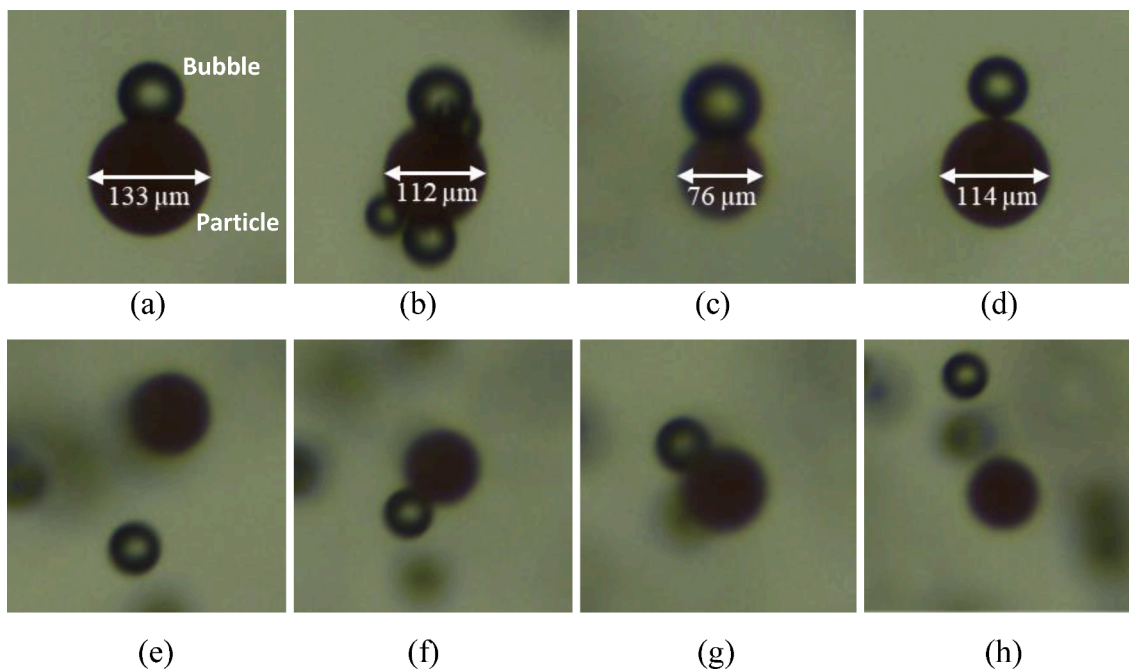
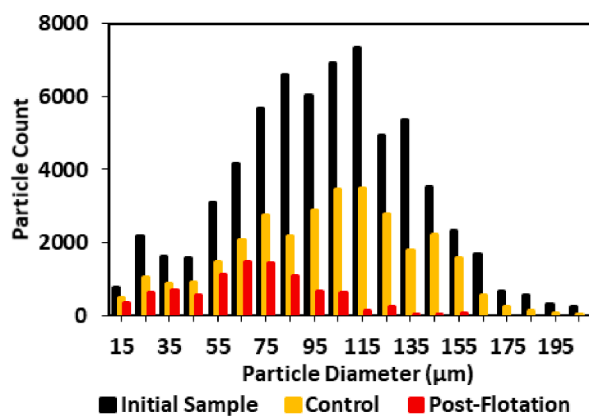


Fig. 5. (a-d) Images of microbubble-spherical PE microparticle aggregates rising in solution, (e-f) bubble particle collision with subsequent attaching and detaching of spherical PE MP particle of diameter 79 μm . Images were captured at 15 frames per second.

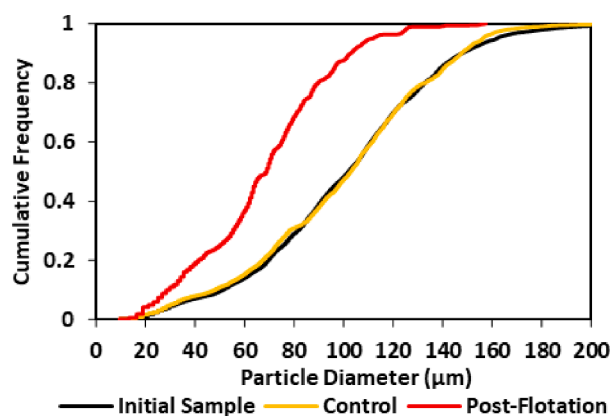
Table 1

Effect of particle density and CMC Tween-20 surfactant on the removal of spherical PE MP. *Relative velocity calculated to that of a 75 μm diameter air bubble rising according to Stokes law in 20 $^{\circ}\text{C}$ water. Measured size distribution for each range is provided in Fig. S2. Approximate bubble density 7500–10,000 bubbles mL^{-1} and 3750–5000 at 1:1 dilution and 3:1 dilution, respectively.

Size range of particles (μm)	MP Dosing (g L^{-1})	Dilution Ratio	CMC Tween 20	MP Particle Density (g cm^{-3})	Relative Velocity* (m s^{-1})	Removal %
113.5 \pm 7.5	0.5	3:1	0.18	0.960	2.55×10^{-3}	84.7
113.5 \pm 7.5	0.5	3:1	0.18	0.995	2.79×10^{-3}	80.6
113.5 \pm 7.5	0.5	3:1	0.18	1.050	3.18×10^{-3}	65.7
113.5 \pm 7.5	0.5	3:1	0.12	0.995	2.79×10^{-3}	90.3
113.5 \pm 7.5	0.5	3:1	0.36	0.995	2.79×10^{-3}	73.2
75.6 \pm 4.5	0.5	1:1	0.12	0.995	2.80×10^{-3}	89.7
75.6 \pm 4.5	0.5	1:1	0.36	0.995	2.80×10^{-3}	63.7



(a)



(b)

Fig. 6. (a) Spherical PE MP size distribution (bin size = $\pm 5 \mu\text{m}$) and (b) normalised cumulative frequency of particle size in initial sample, control sample and post-flotation sample at 1:1 dilution (approximate bubble density 7500–10,000 bubbles mL^{-1}).

106–125 μm and 63–75 μm size ranges, respectively. Higher surfactant concentration increases the wettability of the MP particles, while reducing hydrophobicity [52]. This results in a decrease of attractive hydrophobic forces between particles and bubbles and an increase in the critical separation at which film rupture occurs (Section 3). Particles are therefore less likely to attach at the water–air interface of MB surfaces and attachment efficiency is decreased.

4.4. Effect of particle size on flotation

To investigate particle size-distribution changes by flotation and differences in removal at different particle sizes, tests were carried with a wide-size range of spherical PE samples (10–200 μm ; 995 kg m^{-3} ; standard normal distribution). Fig. 6 shows size distribution analysis based on particle count (Fig. 6a) as well as a normalized cumulative frequency plots (Fig. 6b) for the initial (undiluted sample), the control (diluted sample) and post-flotation samples. The size distribution of the control and the initial sample was similar, indicating that the transfer and dilution of sample solution during experimentation does not lead to a significant change in particle size distribution (Fig. 6b). The decreased particle count seen in the control sample compared to the initial sample (Fig. 6a) is due to dilution. The initial and control samples consisted of particles with 90% of particle diameters in the range 30–160 μm . The post-flotation sample consisted of particles with 90% of particle diameters in the range 25–110 μm . Flotation therefore resulted in a shift of size distribution towards smaller diameters with almost complete removal of particles > 110 μm . Little removal was observed for particles < 70 μm and appeared to be negligible but was difficult to assess due few particles below < 60 μm present in the initial samples. Fig. 6 shows no confidence intervals but comparative measurements of four separately prepared initial samples showed a mean particle count error of 17% in each bin for a size range of 40–170 μm (Fig. S3). Particles outside this range, exhibited greater % error due to low mean particle counts.

To understand the effect of particle size and extent of MB solution addition on MP removal, triplicate experiments were conducted at 1:1 and 3:1 dilution at five narrower MP size ranges of 59.1 ± 5.3 , 75.6 ± 4.5 , 113.5 ± 7.5 , 163.5 ± 10.2 and 551.8 ± 19.4 μm (Fig. 7). Measured size distribution for each range is provided in Fig. S3. Dosing of the initial samples was kept consistent at 0.4–0.5 g L^{-1} . This resulted in

constant plastic volume per volume of MP suspension of approximately 0.5 ml L^{-1} , giving a solid to air volume ratio of approximately 1:10 for 1:1 dilution flotation and solid to air volume ratio of approximately 1:5 for 3:1 dilution flotation, whilst particle concentration decreased with increasing particle size (Table S5). The maximum initial solution particle concentration was 3726 particles mL^{-1} for particles 59.1 ± 5.3 μm , which is well below MB number density of the used MB solution.

The effect of varying particle concentration was tested with particles of mean diameter 75.6 ± 4.5 μm at 0.1 and 0.5 g L^{-1} dosing and particles of mean diameter 163.5 ± 10.2 μm at 0.5 and 2.0 g L^{-1} MP dosing (Table S6). For both particle sizes, variation in MP dosing did not result in significant deviation in removal %. With the mean removal % at both dosing conditions for both particle size ranges remaining within 4% or one standard deviation.

The largest particles with size 551.8 ± 19.4 μm were readily visible by naked-eye and complete removal was verified by visual observation. Removal increased with increasing particle size resulting in full removal at and above 163.5 ± 10.2 μm for both 1:1 and 3:1 dilution. At increased addition of MB solution, removal is increased through increasing interception due to the presence of more bubbles per volume. Higher bubble number density also provides better removal performance at smaller particle sizes, partially compensating for decreasing collision efficiency with decreasing particle size. However, for both dilution ratios, removal performance decreased markedly for the 59.1 ± 5.3 μm size range, which is at the lower end of the diameter range (59–113 μm) of the MBs used (Fig. 4).

Extrapolating the overall trend in removal towards smaller particle sizes would show negligible removal for particle diameter \ll bubble diameter, resulting in an s-shaped removal curve across particle size. Removal increases rapidly at particle diameter \approx bubble diameter with a left-shifted steeper and earlier increase for higher addition of MB solution but similar endpoints for high and low addition of MB solution. This concurs with previous work showing that the optimum bubble diameter for flotation is similar or slightly smaller than the target particle diameter [41,43,65]. A study with particle sizes of 10–50 μm (flocs) and 10–50 μm -sized bubbles showed similar removal trends as observed here, including a rapid increase in removal efficiency with increasing particle size, followed by levelling off as particle size further increased [65].

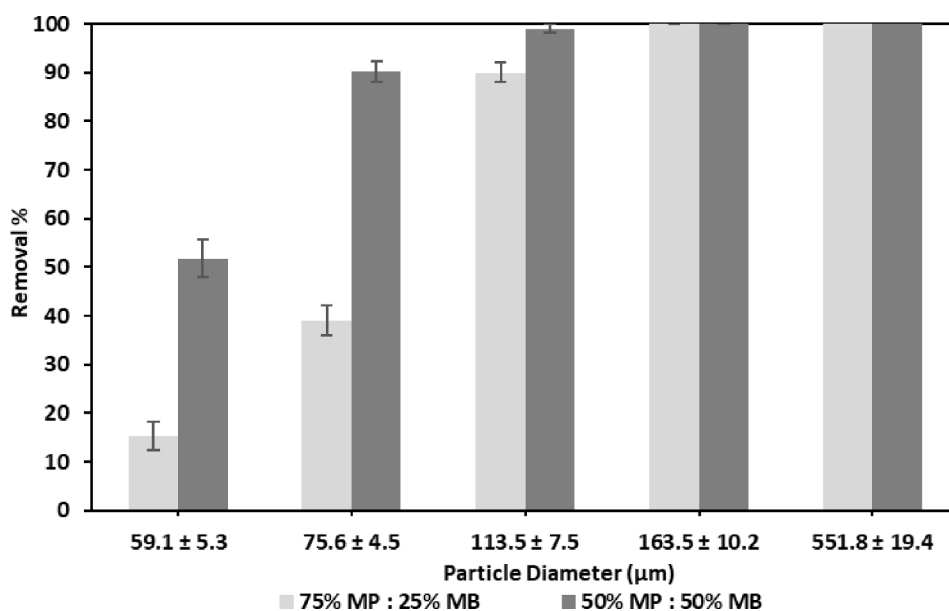


Fig. 7. Removal % of spherical PE MP particles at 3:1 and 1:1 dilution. Error bars represent the standard deviation of triplicate measurements. Particle size given as the mean recorded particle diameter \pm 1 standard deviation of the recorded particle diameters. Approximate bubble density 7500–10,000 bubbles mL^{-1} and 3750–5000 at 1:1 dilution and 3:1 dilution, respectively.

Changes observed in removal with increasing particle size and different MB dilutions can be explained by the different bubble-particle interactions outlined in Fig. 3. Increasing particle size results in increased interception due to the larger projection area of particles and increased collision efficiency due to decreased deflection of the particle around rising bubbles [43]. Attachment efficiency and detachment rate is less affected as gravitational and inertial forces remain small for neutrally buoyant particles in the given size range [58]. This results in a net increase in removal at increasing particle size. Note that due to the near neutral buoyancy of the MP particles used, larger particle size does not greatly increase settling velocity, while for particles with much higher density than water, collision efficiency would decrease due to higher settling velocity resulting in deflection of bubbles [43].

4.5. Flotation of non-spherical microplastics

To study bubble interactions with non-spherical MP particles with rough surfaces and to investigate differences between different types of plastic, flotation experiments were conducted with irregular shaped PE, PP, PVC and PMMA particles with densities of 0.955, 0.905, 1.380 and 1.180 g cm⁻³ respectively, obtained from sanding (see Methods section). Fig. 8 shows aspect ratios and size distribution in control and post-flotation samples. Aspect ratio distribution of all four plastic types is provided in Fig. S4 showing that most particles fell within an aspect ratio of 1–2 (>70%) and 2–3 (>15%). Note, while Fig. 8 shows occurrence of aspect ratios beyond 4 these were negligible for total particle count. Prior to flotation, all four plastic types had similar aspect ratios and size distributions. In comparison to the commercial spherical PE particles used (Figs. S2 and S3), all four control samples of sanded plastic particles exhibited a skewed size distribution towards smaller sizes, with a large portion of particles < 50 μm. This was more pronounced for PVC and PMMA which had 56% and 62% of particles < 50 μm, respectively. PE and PP on the other hand had 36% and 39% of particles < 50 μm, respectively.

Fig. 8 (a, c, e, g) illustrates that for a given particle size, flotation preferentially removed particles with higher aspect ratio. Size-related removal performance for the four different types of plastic was similar as indicated by similar size distributions after flotation (Fig. 8 b, d, f, h). Total particle removal percentage for PE, PP, PVC and PMMA was 83%, 79%, 66% and 83% respectively, indicating that PVC with the highest density of 1.38 g cm⁻³ and a high proportion (56%) of particles < 50 μm was the most difficult to remove. Interestingly PMMA, which also has a density higher than water and a high proportion of particles < 50 μm, achieved similarly high removal % to both PE and PP. This could partially be due to the lower magnitude zeta potential of PMMA over all pH compared to PE, PP and PVC which had similar zeta potentials (Fig. S5). This may subject PMMA particles to lower electrostatic repulsive forces when interacting with MBs and could counteract increased hydrodynamic repulsion due to higher relative velocities. Importance of zeta potential is further discussed in the next section. Pre-flotation size distribution of PE showed a slightly higher percentage (52%) of particles above 60 μm compared to PP, PVC and PMMA which had 24–44% of particles above 60 μm. This may have caused the highest removal of PE, despite its density not being the lowest as almost all particles above 60 μm were seen to be removed for all four plastics.

Beyond minor differences in total removal, all four plastic types provide a similar flotation performance with almost 100% removal rates at particle sizes above 70 μm and average removal rates of 65–84% between 20 and 70 μm (Fig. S6). For the size range of 50–60 μm, removal ranged from 83 to 90%, which was markedly different than removal of similar-sized spherical MP particles (52% at 59.1 ± 5.3 μm) and same MB dilution (Fig. 8). The increased removal for non-spherical irregularly shaped MP indicates that such particles attach more readily with rising MBs than spherical particles with an equivalent cross section.

Preferential removal of irregularly shaped MP can be partially explained by the greater likelihood of interception for elongated

particles with bubbles. Irregularly shaped particles have a higher surface area to volume ratio compared to spherical particles which increases surface drag force and slows particle movement. This effect has previously been shown to reduce deflection and increase collision efficiency of rough and to a greater extent irregular shaped glass particles (100–200 μm) travelling towards static bubbles (1.6 mm) [54]. In addition, previous research showed that attachment efficiency is increased for irregular glass particles (75–90 μm) sliding along the surface of a bubble (1.56 mm) by an order of magnitude compared to spherical particles. This is due to protruding edges on the rough irregular particles effectively reducing separation between particle and bubble surface and more easily triggering film rupture and the formation of a three phase wetting perimeter [66–68]. Results of this study indicate that the previously shown increase in collision and attachment efficiency leading to higher removal of rough and irregular shaped particles by mm sized bubbles, are also applicable to MP particles and micrometer-sized bubbles.

4.6. Effect of salt addition on MB flotation

Electrostatic forces are important for MB and MP interaction as repulsive or attractive forces play a role in particle-bubble trajectory and therefore collision efficiency. Zeta potential is a measure of the magnitude of electrostatic force due to particle/bubble surface charge. The zeta potential of 75.6 ± 4.5 μm spherical PE particles were –2 mV at pH 3 and –78 mV at pH 7.5 (Fig. S6). The typical zeta potential of MBs in DI water is approximately –35 mV in DI water and decreasing with increasing ionic strength (–5 mV at 10⁻² (mol L⁻¹) MgCl₂) [43,46]. Increasing salt concentration from 1 mM to 50 mM (KCl was used, see Text S1), reduced the zeta potential of PE MP particles from –90 mV to –52 mV at pH ≈ 7.5 (Fig. S6). A similar decrease of 40–50% was also observed for other pH tested. The reduction of zeta potential for both MP particles and MBs is due a compression of the Debye layer, that reduces the distance over which surface charge exerts its force (Debye screening) [62]. Both MP particles and MBs have negative zeta potentials and mutual repulsive electrostatic forces decrease their collision efficiency. Increasing the ionic strength of solution by salt addition should lead to a decrease in repulsive electrostatic forces.

To evaluate the effect of electrostatic forces on MP removal, flotation experiments at different ionic strength using NaCl, MgCl₂, Al₂(SO₄)₃ and AlK(SO₄)₂ with spherical PE particles (59.1 ± 5.3 μm) were conducted (Fig. 9). For all salts, removal increased from a baseline removal of 15% with DI water to a maximum of approximately 60–65%. NaCl and MgCl₂ addition resulted in a similar increase in removal with increasing ionic strength, indicating little difference between adding monovalent or bivalent salts. Al₂(SO₄)₃ addition resulted in ~ 60% removal at a much lower ionic strength of 2.4 × 10⁻⁴ mol L⁻¹ Al₂(SO₄)₃ compared to ~ 60% removal at 1.7 × 10⁻² mol L⁻¹ NaCl and 3.1 × 10⁻² mol L⁻¹ MgCl₂. In comparison, both NaCl and MgCl₂, at similar ionic strengths, reach a removal percentage of approximately 15–20%. An additional test was done with AlK(SO₄)₂ to see if it also resulted in enhanced removal compared to NaCl and MgCl₂. Results showed a removal of 57% with AlK(SO₄)₂ at 1.9 × 10⁻³ mol L⁻¹, whereas NaCl and MgCl₂ showed 40–45% removal at similar ionic strengths. This indicated that alum salts in general perform better at increasing removal. The increased effectiveness of alum salts is not unexpected as these are promoters of flocculation processes [36,69,70]. Investigations have previously shown enhanced adsorption of Al³⁺ ions compared to other ions onto kaolinite surfaces has been previously observed and attributed to high electro-negativity and weak pairing ability with chloride ions [71].

Results indicated that all salts were able to effectively reduce Debye length of both MBs and MP particles, decreasing the separation distance over which repulsive electrostatic forces act and increasing collision efficiency by increasing importance of short-distance attractive van der Waals and long distance attractive hydrophobic forces. Modelling for neutrally buoyant particles showed that an increase in dimensionless

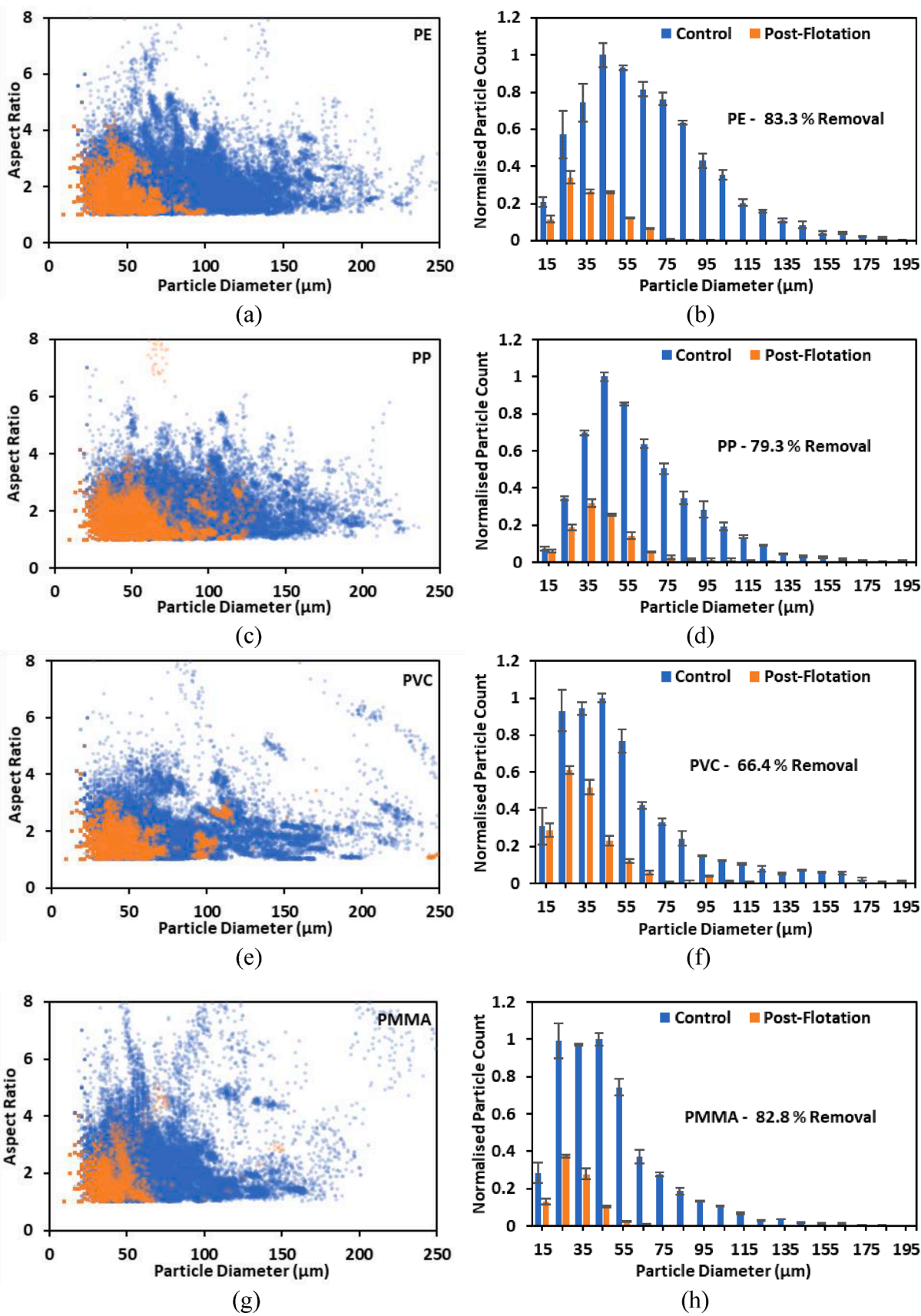


Fig. 8. Aspect ratio (a, c, e, g) and size distribution (bin range = $\pm 5 \mu\text{m}$) (b, d, f, h) of irregular shaped MP particles, control sample (blue) and the post-flotation sample (orange) at 1:1 dilution, approximate bubble density 7500–10,000 bubbles mL^{-1} . Error bars represent standard deviation in particle counts; (a), (b) – PE, (c), (d) – PP, (e), (f)– PVC, (g), (h) – PMMA.

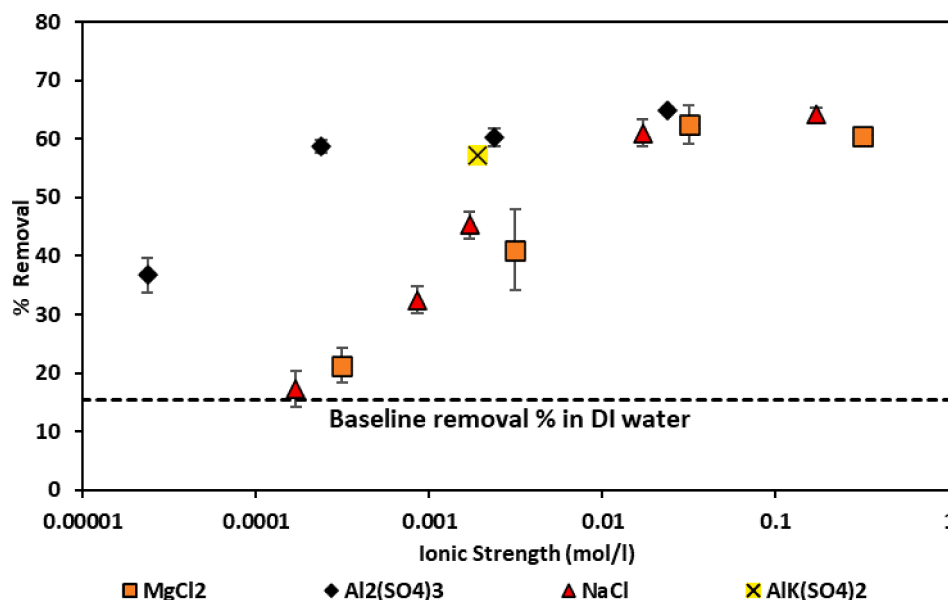


Fig. 9. Removal of PE MP particles sized $60.5 \pm 4.1 \mu\text{m}$ at 1:3 dilution (approximate bubble density $3750\text{--}5000 \text{ bubbles mL}^{-1}$) different NaCl, MgCl₂, Al₂(SO₄)₃, AlK(SO₄)₂ concentrations. The dotted line represents the baseline removal in DI water with no added salt. Error bars represent the standard deviation of triplicate experiments.

inverse Debye length Kr from 10^2 to 10^4 , leads to an increase in collision efficiency by a factor of 6 from approximately 0.04 to 0.25 [43]. In comparison, Fig. 9 shows an increase in removal by a factor of 4 from 15% to 60%. Ionic strength indicates that the dimensionless inverse Debye length Kr , for particles of radius $r = 30 \mu\text{m}$, increases from ≈ 480 to 15,000 for the alum salts and from $\approx 1,400$ to 50,000 for NaCl and MgCl₂. Exact values for each salt can be seen in Table S4. In addition to an increase in the collision efficiency, a decrease in the repulsive electrostatic forces acting between particles and bubbles could lead to a greater chance of attractive interparticle forces capturing particles via contactless flotation which would be perceived as an increased attachment efficiency. Another factor considered was the effect of salinity on the behavior of MBs in solution. The presence of 38 g kg^{-1} of salt in seawater has been shown to cause a 1%, 3%, and 8% increase in water surface tension, density and dynamic viscosity, respectively [72]. Calculations using Equation (2), show that MBs would have rise velocities 4.6% lower in seawater than in saltwater. Theoretically this could result in increased collision efficiencies as there would be smaller repulsive hydrodynamic forces between rising MBs and particles. Investigations however showed that these changes in water properties did not have a major impact on the designs needed for industrial DAF treatment of sea water [72]. It is therefore unlikely that the salt additions, with maximum dose of 10 g L^{-1} of salt, had any significant effect on flotation performance. Additionally, MB size distribution was purposely kept consistent throughout all experiments by using only DI water in the MB generator. Therefore, changes in removal % is only due to the presence of salt ions in the MP suspension and its effect on MP and MB surface properties previously discussed. Additional testing with irregular sanded PE, PP, PVC and PMMA was done with 0.17 mol L^{-1} NaCl. A key conclusion was that the already increased removal % of rough irregular MP in RO water limits the improvement in removal % when salt is added. Detailed discussion and figures related to these results can be found in supporting information (Text S3, Table S7, Fig. S7).

4.7. Applicability of experimental method and image analysis

The approach described in this manuscript for performing and assessing removal % of MP particles consisted of four key aspects, MB generation via regenerative turbine pump, batch flotation in a flotation column, in-situ image capture of MP particles and analysis of images

with in-house MATLAB code. In a previous publication, the merits of MB generation via regenerative turbine pump and in-situ image analysis of MB populations are discussed and detailed investigations of MB characteristics are carried out [55]. Assessment of microbubble flotation performance of particulates and particulate presence in solution can be done in a variety of ways (Tables S1 & S2). In-situ methods include measurement of solution turbidity change, absorbance measurements, and laser particle analysis [44,45,47,51]. These methods either do not allow for detailed measurements of particle size distributions or would typically require verification of measured particle sizes by additional image analysis. Other methods rely on recovery of solid particulates and measurement via either gravimetric methods or microscopic analysis [73-75], both of which are time consuming and as shown through validation of our method in supporting information (Text S2), physical separation of solids from solution results in loss of particulates unrelated to flotation performance. The experimental setup used for in-situ image capturing in our work has been shown to allow quickly repeatable measurement of both MB and MP particulate sizes and concentrations, and even allowed for capture of MB-MP interaction, all without the need for major changes in experimental setup. The use of in-house MATLAB code allows for easy tailoring of image analysis to accurately characterise MBs and different particulate types.

The batch flotation and in-situ image analysis methodology presented was designed to optimise accurate quantification of MP removal from water. As a result, conditions were different in certain aspects to those present in real world DAF applications. For example, the presence of large quantities of other contaminants and solid particles in wastewater treatment was not replicated. The use of a batch operated flotation column differs from the continuously operated flotation tanks present in industry, in which internal geometry has a significant effect on flotation performance [76]. Additionally, not all parameters which will affect removal rate in real world applications were varied. Whilst this work has already investigated the effects of MB characteristics, MP particle characteristics, salinity and surfactant concentration, studies have shown that other parameters such as influent viscosity, temperature, pH, surface tension, solid content, and organic matter will all have an effect on the MB characteristics as well as flotation performance [77-79]. Further work on analyzing MP removal in lab scale continuous flotation tanks with a greater range of solution types, including industrial waste streams, and further variation and measurement of parameters would

aid in further understanding of real-world removal of MP particles. The work may also focus on visualizing collisional interaction of particles and bubbles.

5. Conclusions

An in-situ batch tracking and analysis method for determining microbubble (MB) and microplastic (MP) concentration, size and shape distribution via image capturing in a viewing slit was developed. The method allows real time monitoring of particle-bubble interaction at the micro scale and straightforward comparison of MP particle concentration before and after flotation. Tests at different liquid phase surfactant concentrations, MP size distributions and density with both spherical PE and non-spherical PE, PP, PVC and PMMA particles showed that differences in removal efficiency could be rationalized by theoretical knowledge. MP behaviour and removal efficiency is comparable to MB flotation of non-plastic particles. Non-spherical MP with varied aspect ratios (1–3; >90%) show that flotation preferentially removed particles with higher aspect ratio due to greater likelihood of bubble interception for elongated particles. Differences in removal efficiency, specifically for PMMA, was attributed to lower zeta potential leading to decreased electrostatic repulsion of bubbles and particles and increased attachment efficiency. Increased removal due to decreased zeta potential, could be also shown at increased ionic strength of the aqueous phase.

Declaration of Competing Interest

The authors declare that they have no known competing financial interests or personal relationships that could have appeared to influence the work reported in this paper.

Data availability

Data will be made available on request.

Acknowledgements

B.S was supported by a scholarship of the Water Informatics, Science and Engineering (WISE) Centre for Doctoral Training (CDT), funded by the UK Engineering and Physical Sciences Research Council, Grant No. EP/L016214/1.

Appendix A. Supplementary data

Supplementary data to this article can be found online at <https://doi.org/10.1016/j.cej.2022.137866>.

References

- [1] X. Guo, J. Wang, The chemical behaviors of microplastics in marine environment: A review, *Mar. Pollut. Bull.* 142 (2019) 1–14.
- [2] A.L. Andrady, Microplastics in the marine environment, *Mar. Pollut. Bull.* 62 (8) (2011) 1596–1605.
- [3] M. Cole, P. Lindeque, C. Halsband, T.S. Galloway, Microplastics as contaminants in the marine environment: A review, *Mar. Pollut. Bull.* 62 (12) (Dec. 2011) 2588–2597, <https://doi.org/10.1016/j.marpolbul.2011.09.025>.
- [4] A. Cincinelli, C. Scopetani, D. Chelazzi, E. Lombardini, T. Martellini, A. Katsoyiannis, M.C. Fossi, S. Corsolini, Microplastic in the surface waters of the Ross Sea (Antarctica): Occurrence, distribution and characterization by FTIR, *Chemosphere* 175 (2017) 391–400, <https://doi.org/10.1016/j.chemosphere.2017.02.024>.
- [5] Z. Akdogan, B. Guven, Microplastics in the environment: A critical review of current understanding and identification of future research needs, *Environ. Pollut.* 254 (2019) 113011.
- [6] D. Eerkes-Medrano, R.C. Thompson, D.C. Aldridge, Microplastics in freshwater systems: A review of the emerging threats, identification of knowledge gaps and prioritisation of research needs, *Water Res.* 75 (2015) 63–82.
- [7] S. Rezaei, J. Park, M. Fadhil, M. Din, S. Mat Taib, A. Talaiekhazani, K.K. Yadav, H. Kamyab, Microplastics pollution in different aquatic environments and biota: A review of recent studies, *Mar. Pollut. Bull.* (2018), <https://doi.org/10.1016/j.marpolbul.2018.05.022>.
- [8] B. Gewert, M. Ogonowski, A. Barth, M. MacLeod, Abundance and composition of near surface microplastics and plastic debris in the Stockholm Archipelago, Baltic Sea, *Mar. Pollut. Bull.* 120 (1–2) (2017) 292–302, <https://doi.org/10.1016/j.marpolbul.2017.04.062>.
- [9] I.A. Kane, M.A. Clare, E. Miramontes, R. Wogelius, J.J. Rothwell, P. Garreau, F. Pohl, Seafloor microplastic hotspots controlled by deep-sea circulation, *Science* 368 (6495) (2020) 1140–1145.
- [10] S.L. Wright, R.C. Thompson, T.S. Galloway, The physical impacts of microplastics on marine organisms: A review, *Environ. Pollut.* 178 (2013) 483–492.
- [11] J. Wang, C. Peng, H. Li, P. Zhang, X. Liu, The impact of microplastic-microbe interactions on animal health and biogeochemical cycles: A mini-review, *Sci. Total Environ.* 773 (Jun. 2021), 145697, <https://doi.org/10.1016/J.SCITOTENV.2021.145697>.
- [12] A.A. Koelmans, A. Bakir, G.A. Burton, C.R. Janssen, Microplastic as a Vector for Chemicals in the Aquatic Environment: Critical Review and Model-Supported Reinterpretation of Empirical Studies, *Environ. Sci. Technol.* 50 (7) (Apr. 2016) 3315–3326, https://doi.org/10.1021/ACS.EST.5B06069/SUPPL_FILE/ES5B06069_SI_001.PDF.
- [13] L. Hermabessiere, A. Dehaut, I. Paul-Pont, C. Lacroix, R. Jezequel, P. Soudant, G. Duflos, Occurrence and effects of plastic additives on marine environments and organisms: A review, *Chemosphere* 182 (Sep. 2017) 781–793, <https://doi.org/10.1016/J.CHEMOSPHERE.2017.05.096>.
- [14] S. Anbumani, P. Kakkur, Ecotoxicological effects of microplastics on biota: a review, *Environ. Sci. Pollut. Res.* 25 (15) (2018) 14373–14396.
- [15] I.A. Ricardo, E.A. Alberto, A.H. Silva Júnior, D.L.P. Macuvele, N. Padoim, C. Soares, H. Gracher Riella, M.C.V.M. Starling, A.G. Trovó, A critical review on microplastics, interaction with organic and inorganic pollutants, impacts and effectiveness of advanced oxidation processes applied for their removal from aqueous matrices, *Chem. Eng. J.* 424 (2021) 130282.
- [16] A.A. Horton, A. Walton, D.J. Spurgeon, E. Lahive, C. Svendsen, Microplastics in freshwater and terrestrial environments: Evaluating the current understanding to identify the knowledge gaps and future research priorities, *Sci. Total Environ.* 586 (2017) 127–141.
- [17] J. Boucher, D. Friot, Primary Microplastics in the Oceans; a Global Evaluation of Sources, IUCN (2017), <https://doi.org/10.2305/IUCN.CH.2017.01.en>.
- [18] F. De Falco, E. Di Pace, M. Cocca, M. Avella, The contribution of washing processes of synthetic clothes to microplastic pollution, *Sci. Rep.* 9 (1) (Dec. 2019) 1–11, <https://doi.org/10.1038/s41598-019-43023-x>.
- [19] I. Efimova, M. Bagaeva, A. Bagaev, A. Kileso, and I. P. Chubarenko, “Secondary Microplastics Generation in the Sea Swash Zone With Coarse Bottom Sediments: Laboratory Experiments,” *Front. Marine Sci.*, vol. 5, no. SEP, p. 313, Sep. 2018, doi: 10.3389/fmars.2018.00313.
- [20] S. Serranti, R. Palmieri, G. Bonifazi, A. Cózar, Characterization of microplastic litter from oceans by an innovative approach based on hyperspectral imaging, *Waste Manage.* 76 (Jun. 2018) 117–125, <https://doi.org/10.1016/j.wasman.2018.03.003>.
- [21] A. Kunz, B.A. Walther, L. Löwemark, Y.C. Lee, Distribution and quantity of microplastic on sandy beaches along the northern coast of Taiwan, *Mar. Pollut. Bull.* 111 (1–2) (Oct. 2016) 126–135, <https://doi.org/10.1016/j.marpolbul.2016.07.022>.
- [22] A. Gauci, A. Deidun, J. Montebello, J. Abela, F. Galgani, Automating the characterisation of beach microplastics through the application of image analyses, *Ocean Coast. Manag.* 182 (2019) 104950.
- [23] L. Frère, I. Paul-Pont, J. Moreau, P. Soudant, C. Lambert, A. Huvet, E. Rinnert, A semi-automated Raman micro-spectroscopy method for morphological and chemical characterizations of microplastic litter, *Mar. Pollut. Bull.* 113 (1–2) (Dec. 2016) 461–468, <https://doi.org/10.1016/j.marpolbul.2016.10.051>.
- [24] E. Uurasjärvi, S. Hartikainen, O. Setälä, M. Lehtiniemi, A. Koistinen, Microplastic concentrations, size distribution, and polymer types in the surface waters of a northern European lake, *Water Environ. Res.* 92 (1) (Jan. 2020) 149–156, <https://doi.org/10.1002/WER.1229>.
- [25] J. Talvitie, A. Mikola, A. Koistinen, O. Setälä, Solutions to microplastic pollution Removal of microplastics from wastewater effluent with advanced wastewater treatment technologies, *Water Res.* 123 (2017) 401–407, <https://doi.org/10.1016/j.watres.2017.07.005>.
- [26] S. Ziajahromi, P.A. Neale, I. Telles Silveira, A. Chua, F.D.L. Leusch, An audit of microplastic abundance throughout three Australian wastewater treatment plants, *Chemosphere* 263 (2021) 128294.
- [27] K. Waldschläger, S. Lechthaler, G. Stauch, H. Schüttrumpf, The way of microplastic through the environment – Application of the source-pathway-receptor model (review), *Sci. Total Environ.* 713 (2020) 136584.
- [28] M. Enfrin, L.F. Dumée, J. Lee, Nano/microplastics in water and wastewater treatment processes – Origin, impact and potential solutions, *Water Res.* 161 (2019) 621–638.
- [29] Z. Zhang, Y. Chen, Effects of microplastics on wastewater and sewage sludge treatment and their removal: A review, *Chem. Eng. J.* 382 (2020) 122955.
- [30] S. Magni, A. Binelli, L. Pittura, C.G. Avio, C. Della Torre, C.C. Parenti, S. Gorbi, F. Regoli, The fate of microplastics in an Italian Wastewater Treatment Plant, *Sci. Total Environ.* 652 (2019) 602–610.
- [31] K. Conley, A. Clum, J. Deepe, H. Lane, B. Beckingham, Wastewater treatment plants as a source of microplastics to an urban estuary: Removal efficiencies and loading per capita over one year, *Water Research X* 3 (Apr. 2019), 100030, <https://doi.org/10.1016/j.wroa.2019.100030>.
- [32] S. Khuntia, S.K. Majumder, P. Ghosh, Microbubble-aided water and wastewater purification: a review, *Rev. Chem. Eng.* 28 (4–6) (Jan. 2012) 191–221, <https://doi.org/10.1515/revce-2012-0007>.

- [33] E.N. Peleka, G.P. Gallios, K.A. Matis, A perspective on flotation: a review, *J. Chem. Technol. Biotechnol.* 93 (3) (Mar. 2018) 615–623, <https://doi.org/10.1002/jctb.5486>.
- [34] H. Shent, R.J. Pugh, E. Forsberg, A review of plastics waste recycling and the flotation of plastics, *Resour. Conserv. Recycl.* 25 (2) (Feb. 1999) 85–109, [https://doi.org/10.1016/S0921-3449\(98\)00017-2](https://doi.org/10.1016/S0921-3449(98)00017-2).
- [35] C.-Q. Wang, H. Wang, J.-G. Fu, Y.-N. Liu, Flotation separation of waste plastics for recycling—A review, *Waste Manage.* 41 (2015) 28–38.
- [36] J.K. Edzwald, Dissolved air flotation and me, *Water Res.* 44 (7) (Apr. 2010) 2077–2106, <https://doi.org/10.1016/j.watres.2009.12.040>.
- [37] D. Tao, Role of Bubble Size in Flotation of Coarse and Fine Particles—A Review, *Sep. Sci. Technol.* 39 (4) (Jan. 2005) 741–760, <https://doi.org/10.1081/SS-120028444>.
- [38] B. Lin, B. Recke, J.K.H. Knudsen, S.B. Jørgensen, Bubble size estimation for flotation processes, *Miner. Eng.* 21 (7) (Jun. 2008) 539–548, <https://doi.org/10.1016/j.mineng.2007.11.004>.
- [39] N. Ahmed, G.J. Jameson, The effect of bubble size on the rate of flotation of fine particles, *Int. J. Miner. Process.* 14 (3) (Apr. 1985) 195–215, [https://doi.org/10.1016/0301-7516\(85\)90003-1](https://doi.org/10.1016/0301-7516(85)90003-1).
- [40] D.M. Leppinen, A kinetic model of dissolved air flotation including the effects of interparticle forces, *J. Water Suppl. Res. Technol.-Aqua* 49 (5) (Aug. 2000) 259–268, <https://doi.org/10.2166/aqua.2000.0022>.
- [41] M.Y. Han, Modeling of DAF: the effect of particle and bubble characteristics, *J. Water Supply: Res. Technol.-Aqua* 51 (1) (Feb. 2002) 27–34, <https://doi.org/10.2166/aqua.2002.0003>.
- [42] S. Dockko, M.Y. Han, Fundamental characteristics of bubbles and ramifications for the flotation process, *Water Sci. Technol.* 50 (12) (Dec. 2004) 207–214, <https://doi.org/10.2166/wst.2004.0715>.
- [43] D.M. Leppinen, Trajectory analysis and collision efficiency during microbubble flotation, *J. Colloid Interface Sci.* 212 (2) (Apr. 1999) 431–442, <https://doi.org/10.1006/jcis.1998.6075>.
- [44] R.J. Gochin, J. Solari, The role of hydrophobicity in dissolved air flotation, *Water Res.* 17 (6) (Jan. 1983) 651–657, [https://doi.org/10.1016/0043-1354\(83\)90234-8](https://doi.org/10.1016/0043-1354(83)90234-8).
- [45] M. Han, S. Dockko, Zeta potential measurement of bubbles in DAF process and its effect on the removal efficiency, *KSCSE J. Civ. Eng.* 2 (4) (Dec. 1998) 461–466, <https://doi.org/10.1007/BF02830128>.
- [46] P. George, A.V. Nguyen, G.J. Jameson, Assessment of true flotation and entrainment in the flotation of submicron particles by fine bubbles, *Miner. Eng.* 17 (7–8) (Jul. 2004) 847–853, <https://doi.org/10.1016/J.MINENG.2004.02.002>.
- [47] J. Hanotu, H.C.H. Bandulasena, W.B. Zimmerman, Microflotation performance for algal separation, *Biotechnol. Bioeng.* 109 (7) (Jul. 2012) 1663–1673, <https://doi.org/10.1002/bit.24449>.
- [48] V. Sarrot, Z. Huang, D. Legendre, P. Guiraud, Experimental determination of particles capture efficiency in flotation, *Chem. Eng. Sci.* 62 (24) (Dec. 2007) 7359–7369, <https://doi.org/10.1016/j.ces.2007.08.028>.
- [49] M.R. Aliff Radzuan, M.A. Abia-Biteo Belope, R.B. Thorpe, Removal of fine oil droplets from oil-in-water mixtures by dissolved air flotation, *Chem. Eng. Res. Des.* 115 (2016) 19–33.
- [50] H. Wang, X.-L. Chen, Y. Bai, C. Guo, L.I. Zhang, Application of dissolved air flotation on separation of waste plastics ABS and PS, *Waste Manage.* 32 (7) (2012) 1297–1305.
- [51] Y. Wang, Y. Li, L. Tian, L. Ju, Y. Liu, The removal efficiency and mechanism of microplastic enhancement by positive modification dissolved air flotation, *Water Environ. Res.* 93 (5) (May 2021) 693–702, <https://doi.org/10.1002/WER.1352>.
- [52] Y. Xing, X. Gui, L. Pan, B.-E. Pinchasik, Y. Cao, J. Liu, M. Kappl, H.-J. Butt, Recent experimental advances for understanding bubble-particle attachment in flotation, *Adv. Colloid Interface Sci.* 246 (2017) 105–132.
- [53] D.I. Verrelli, P.T.L. Koh, A.V. Nguyen, Particle–bubble interaction and attachment in flotation, *Chem. Eng. Sci.* 66 (23) (Dec. 2011) 5910–5921, <https://doi.org/10.1016/J.CES.2011.08.016>.
- [54] B. Vaziri Hassas, H. Caliskan, O. Guven, F. Karakas, M. Cinar, M.S. Celik, Effect of roughness and shape factor on flotation characteristics of glass beads, *Colloids Surf., A* 492 (2016) 88–99.
- [55] B. Swart, Y. Zhao, M. Khaku, E. Che, R. Maltby, Y.M.J. Chew, J. Wenk, In situ characterisation of size distribution and rise velocity of microbubbles by high-speed photography, *Chem. Eng. Sci.* 225 (2020) 115836.
- [56] N. Otsu, Threshold selection method from gray-level histograms, *IEEE Trans Syst Man Cybern* vol. SMC-9, no. 1 (1979) 62–66, <https://doi.org/10.1109/tsmc.1979.4310076>.
- [57] R. (Roland) Clift, J. R. Grace, M. E. Weber, *Bubbles, drops, and particles*. Academic Press, 1978.
- [58] B. V. Derjaguin, S. S. Dukhin, and N. N. Rulyov, “Kinetic Theory of Flotation of Small Particles,” in *Surface and Colloid Science*, Boston, MA: Springer US, 1984, pp. 71–113. doi: 10.1007/978-1-4615-7972-4_2.
- [59] J. Ralston, D. Fornasiero, R. Hayes, Bubble–particle attachment and detachment in flotation, *Int. J. Miner. Process.* 56 (1–4) (Apr. 1999) 133–164, [https://doi.org/10.1016/S0301-7516\(98\)00046-5](https://doi.org/10.1016/S0301-7516(98)00046-5).
- [60] C. E. Brennen, “Fundamentals of multiphase flow,” *Fundamentals of Multiphase Flow*, vol. 9780521848046, pp. 1–345, Jan. 2013, doi: 10.1017/CBO9780511807169.
- [61] V. Sarrot, P. Guiraud, D. Legendre, Determination of the collision frequency between bubbles and particles in flotation, *Chem. Eng. Sci.* 60 (22) (Nov. 2005) 6107–6117, <https://doi.org/10.1016/j.ces.2005.02.018>.
- [62] W. B. Russel, D. A. Saville, W. R. Schowalter, “Colloidal Dispersions,” Dec. 1989, doi: 10.1017/CBO9780511608810.
- [63] R. Etchepare, H. Oliveira, M. Nicknig, A. Azevedo, J. Rubio, Nanobubbles: Generation using a multiphase pump, properties and features in flotation, *Miner. Eng.* 112 (Oct. 2017) 19–26, <https://doi.org/10.1016/J.MINENG.2017.06.020>.
- [64] S. Li, H. Liu, R. Gao, A. Abdurahman, J. Dai, F. Zeng, Aggregation kinetics of microplastics in aquatic environment: Complex roles of electrolytes, pH, and natural organic matter, *Environ. Pollut.* 237 (2018) 126–132.
- [65] M. Han, T. Kim, J. Kim, Effects of floc and bubble size on the efficiency of the dissolved air flotation (DAF) process, *Water Sci. Technol.* 56 (10) (Nov. 2007) 109–115, <https://doi.org/10.2166/wst.2007.779>.
- [66] D.I. Verrelli, W.J. Bruckard, P.T.L. Koh, M.P. Schwarz, B. Follink, Particle shape effects in flotation. Part 1: Microscale experimental observations, *Miner. Eng.* 58 (Apr. 2014) 80–89, <https://doi.org/10.1016/J.MINENG.2014.01.004>.
- [67] J. F. Anfruns, J. A. Kitchener, “Rates of capture of small particles in flotation,” *Transactions of the Institution of Mining and Metallurgy, Section C: Mineral Processing and Extractive Metallurgy*, vol. 86, 1977.
- [68] M. Takahashi, ζ Potential of Microbubbles in Aqueous Solutions: Electrical Properties of the Gas–Water Interface, *J. Phys. Chem. B* 109 (46) (Nov. 2005) 21858–21864, <https://doi.org/10.1021/jp0445270>.
- [69] J.K. Edzwald, J.P. Walsh, G.S. Kaminski, H.J. Dunn, Flocculation and Air Requirements for Dissolved Air Flotation, *Journal - American Water Works Association* 84 (3) (Mar. 1992) 92–100, <https://doi.org/10.1002/j.1551-8833.1992.tb07325.x>.
- [70] M. Graca Rasteiro, P. Sharma, M. Ahammed, A. Blanco, R. Miranda, I. Latour, Understanding the Efficiency of Aluminum Coagulants Used in Dissolved Air Flotation (DAF), *Front. Chem.* 8 (2020) 27, <https://doi.org/10.3389/fchem.2020.00027>.
- [71] A. Doi, M. Khosravi, M. Ejtemaei, T.A.H. Nguyen, A.V. Nguyen, Specificity and affinity of multivalent ions adsorption to kaolinite surface, *Appl. Clay Sci.* 190 (Jun. 2020), 105557, <https://doi.org/10.1016/J.CLAY.2020.105557>.
- [72] J. Haarhoff, J.K. Edzwald, Adapting dissolved air flotation for the clarification of seawater, *Desalination* 311 (Feb. 2013) 90–94, <https://doi.org/10.1016/J.DESAL.2012.10.035>.
- [73] W.J. Shim, S.H. Hong, S.E. Eo, Identification methods in microplastic analysis: a review, *Anal. Methods* 9 (9) (2017) 1384–1391.
- [74] M. Bilgin, M. Yurtsever, F. Karadagli, Microplastic removal by aerated grit chambers versus settling tanks of a municipal wastewater treatment plant, *J. Water Process Eng.* 38 (Dec. 2020), 101604, <https://doi.org/10.1016/j.jwpe.2020.101604>.
- [75] Y. Zhou, B. Albijanic, B. Tadesse, Y. Wang, J. Yang, Investigation of bubble–particle attachment interaction during flotation, *Miner. Eng.* 133 (Mar. 2019) 91–94, <https://doi.org/10.1016/J.MINENG.2018.12.023>.
- [76] V.R. Fanaie, M. Khiadani, T. Ayres, Effects of internal geometry on hydrodynamics of dissolved air flotation (DAF) tank: An experimental study using particle image velocimetry (PIV), *Colloids Surf., A* 575 (Aug. 2019) 382–390, <https://doi.org/10.1016/J.COLSURFA.2019.05.027>.
- [77] N. Rajapakse, M. Zargar, T. Sen, M. Khiadani, Effects of influent physicochemical characteristics on air dissolution, bubble size and rise velocity in dissolved air flotation: A review, *Sep. Purif. Technol.* 289 (2022) 120772.
- [78] J.K. Edzwald, Algae, Bubbles, Coagulants, and Dissolved Air Flotation, *Water Sci. Technol.* 27 (10) (May 1993) 67–81, <https://doi.org/10.2166/WST.1993.0207>.
- [79] V.R. Fanaie, M. Khiadani, Effect of salinity on air dissolution, size distribution of microbubbles, and hydrodynamics of a dissolved air flotation (DAF) system, *Colloids Surf., A* 591 (Apr. 2020), 124547, <https://doi.org/10.1016/J.COLSURFA.2020.124547>.